X CONGRESSO NACIONAL DE ENGENHARIA MECÂNICA 2018
20 A 24 DE MAIO DE 2018 SALVADOR – BA – BRASIL

CONSTRUCTION OF A DEHYDRATOR CHAMBER WITH TEMPERATURE CONTROL

R. P. Menezes Filho, rogeriofilho03@gmail.com[1]

[1]Instituto Federal de Educação, Ciência e Tecnologia Fluminense, R. Dr. Siqueira, 273 – Parque Dom Bosco, Campos dos Goytacazes – RJ

***Abstract**: Dehydration, a well-known and efficient technique for food preservation, can be provided by an equipment known as dehydrator (or dryer), that produces a hot airflow, to which the food is exposed until its water molecules are extracted. However, working temperatures must not exceed certain limits, under risk of denaturation of the exposed food molecules, which implies the need for temperature control. Thus, the objective of this work was to build a dehydration chamber with temperature control that meets the performance requirements for this type of apparatus. In this manner, the project began in the conception and design of the equipment; then the physical parts were machined and fixed to one another, forming the structure, which could then receive the electrical and electronic components; Finally, the system was analyzed from the thermal point of view, i.e. its dynamics were described in mathematical terms, which, through the use of computer simulation tools, was used for the design of the temperature control system. The results from the perspective of the performance of the temperature controller were formidable, so were the dehydration results, which were equivalent or superior to those of the commercially available equipment of this type. In short, the dehydrator chamber was built successfully, maintaining fidelity to the scope from all angles - aesthetic and functional.*

***Keywords:** Dehydrator Chamber, Temperature Control, Dehydration*

1. INTRODUCTION

Food preservation consists in the use of techniques with the aim of preventing food from the growth of unwanted microorganisms. There are numerous methods for this purpose, such as: salting, smoking, cold treatment, heat treatment, alcohol preservation, etc. (Fellers, 1927). In the case of salting and smoking, specifically, the process has the purpose of removing the water molecules from the food, i.e., dehydrating it, which is an effective way of preserving it. Nevertheless, food dehydration is not restricted to the salting technique (Brian, 2002). Drying food by its exposure to the sun and wind is also a dehydration technique. This technique can be employed with the use of an equipment (dehydrator) that provides a flow of hot air along the food surface (Fellows, 2009). The most common food dehydrators on the market are based on this heated airflow principle. Ergo, these machines make use of two primordial actuators: an airflow generator - usually a fan - and a heating element, which is usually a resistor, but even solar power can be used as a source of heat. In some cases, the fan is expendable since the airflow can be created naturally by convection. Since some food, when subjected to certain temperatures, may lose their natural characteristics, a good food dehydrator should offer a function of working temperature adjustment. Additionally, in order to this temperature control be efficient and robust to disturbances, a closed-loop configuration is necessary, since a thermal system like this is very susceptible to external interferences and hard to be modeled with great accuracy. Therefore, the goal of this project is to construct from scratch a dehydrating chamber with temperature control. Its performance must be at least equivalent to the commercial ones.

1.1. Operation Principle

The operating principle of a dehydrator is very simple and intuitive. Hot air circulates through a chamber containing the food you want to dry, carrying the moisture out of it. For this reason, a constant airflow is essential in a dehydrator. In addition, the air must be heated, since higher temperatures promote the combination of water molecules with air. Figure 1 summarizes the operation of a dehydrator using heated airflow.

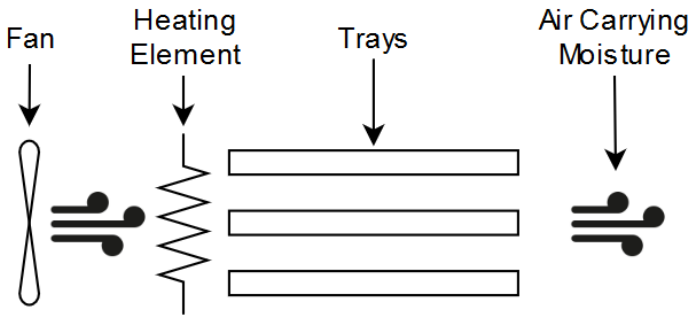

Figure 1. Operation principle of a dehydrator.

The process is similar to drying clothes on a clothesline, which dry faster as temperature and air circulation increase. Likewise, food dehydration is not conceived as an exact science, since every kind of food or material reacts to the process differently. Moreover, there are possible interferences of environmental conditions, such as the relative humidity of air, that directly affects this process, but it is not a variable controlled by this type of equipment (TSM Products, 2011). Unlike dehydration by osmosis, that uses salt or sugar, the dehydration by heat flow, as it is called, depends exclusively on the hot air flow along the surface of the food. In short, there are three key factors regarding dehydration capacity: relative humidity, temperature and velocity of the airflow.

2. CONSTRUCTION

In order to create the proper conditions for dehydration, according to a established design, the physical structure is a box with a total volume of 60 liters, consisting of two 500x330mm aluminum frames, two 500x363mm frames and two other mostly made of steel net, which makes possible the airflow through the chamber, measuring 363x330mm. Inside there are three rails that hold three aluminum trays of 7.72l each, where the food is placed. The aluminum chamber is fixed on a wooden base of 800x400mm, which makes the structure more mechanically robust.

Figure 2. Dehydrator chamber after assembling.

3. ELECTRICAL PROJECT

The electrical circuit of this project is illustrated by Figure 3. The **Arduino Uno** was used in this project as a driver, or data acquisition board. This microcontroller functions only as an interface between the SIMULINK and the sensors and actuators. The **heater** resistor chosen for project was a 2kW fined model, whose characteristics are compatible with the expected working temperatures. Due to the high power of the heating element, it cannot be directly driven by the Arduino, instead it requires a power interface. The power interface chosen was the **Fotek SSR-25A solid-state relay**. This device can be operated with input voltages between 3 and 32VDC, its activation occurs whenever the voltage between the input terminals is greater than 2.4VDC and the deactivation when it is less than 1VDC. The output operates with voltages between 24 and 380VAC. For this application, the input varies between 0 and 5VDC, through a PWM signal. The output ranges from 0, for 0% duty cycle at the input, and 127V, for 100% duty cycle at the input (Fotek, 2016). The **55W Arno fan**, originally a domestic commercial model, was adapted for this application, receiving an aluminum structure. The only sensor used was the **LM35 temperature sensor**, whose application was to provide the temperature measurement and to feed it back into the system, closing the control loop. This sensor works in an analog

way, that is, the output signal varies continuously across the actuation range proportionally to its temperature. In this case, the sensor is powered with 5VDC, so its output signal varies between 0 and 5VDC (Texas Instruments, 2017).

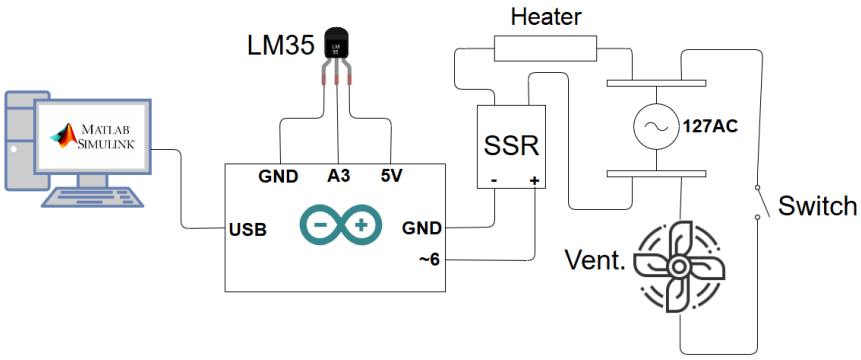

Figure 3. Electrical circuit.

4. THERMAL MODELING

The thermal system of this design can be expressed, in a simplified way, through Figure 4.

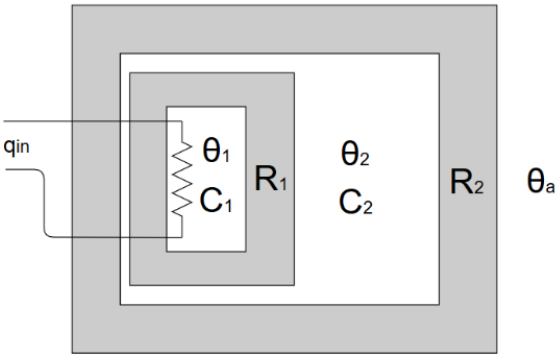

Figure 4. Thermal model.

The thermal resistance R_2, in summary form, refers to the structure of the chamber, including the aluminum plates, the wooden base and the steel net. The thermal resistance R_1 refers to the metal sheath in the heater resistor, the heat generating element, is actually inside this layer. θ_1 is the temperature inside the heater resistor, θ_2 inside the chamber and θ_a is the ambient temperature. C_1 is the thermal capacitance of the interior of the heater resistor and C_2 inside the chamber. Finally, the variable q_{in} is the input of heat through the resistive element, which is located inside the heater resistor. It is expected, in practice, that the parameters relating to the actuator are very different from those of the chamber itself. However, R_1 and C_1 are relevant enough to have an influence on system dynamics (Close et al., 2002). Based equations 1 and 2, the thermal modeling of this system is synthesized by equation 3.

$$\dot{\theta}_1 = \frac{1}{C_1}\left[q_{in}(t) - \frac{1}{R_1}(\theta_1 - \theta_2)\right] \tag{1}$$

$$\dot{\theta}_2 = \frac{1}{C_2}\left[\frac{1}{R_1}(\theta_1 - \theta_2) - \frac{1}{R_2}(\theta_2 - \theta_2)\right] \tag{2}$$

$$\frac{\hat{\Theta}_2(s)}{\hat{Q}_{in}(s)} = \frac{\frac{1}{R_1C_1C_2}}{s^2 + \left(\frac{1}{R_1C_1} + \frac{1}{R_1C_2} + \frac{1}{R_2C_2}\right)s + \frac{1}{R_1C_1R_2C_2}} \tag{3}$$

5. PARAMETER ESTIMATION

Considering the thermal model found in the previous section, the next step is to stimulate the system and observe its behavior. The transfer function (Eq. 3) has its parameters as a function of R_1, R_2, C_1 and C_2, however, these parameters cannot be found individually by the estimation method chosen for this work. Instead, their combinations will be replaced by constants *a*, *b* and *c*, as stated in Eq. 4, 5 and 6. Thus, the transfer function of Eq. 3 can be rewritten as Eq. 7.

$$a = \frac{1}{R_1 C_1 C_2} \tag{4}$$

$$b = \frac{1}{R_1 C_1} + \frac{1}{R_1 C_2} + \frac{1}{R_2 C_2} \tag{5}$$

$$c = \frac{1}{R_1 C_1 R_2 C_2} \tag{6}$$

$$\frac{Y(s)}{U(s)} = \frac{a}{s^2 + bs + c} \tag{7}$$

According to the model, a second order system is expected. Thus, the system was stimulated for 4 times, with steps of 20, 40, 60 and 80% of the maximum voltage, i.e., 25.4; 50.8; 76.2 and 101.6V respectively. The temperature output was observed, as shown in Figure 5. A moving average filter was used, operating as follows: every 500 samples a mean is calculated, which is fixed at the output until the next average (after 500 samples) is calculated.

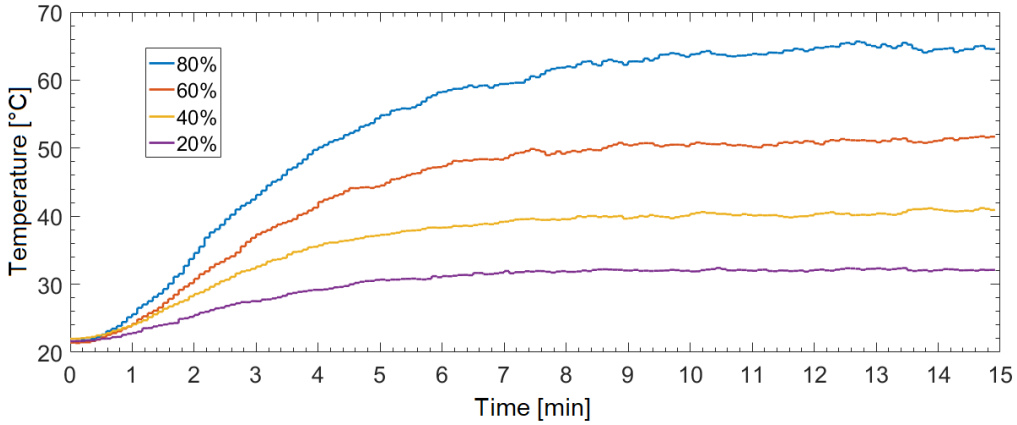

Figure 5. Step response for 20, 40, 60 and 80%.

Analyzing the four different stimulation response curves by four linearly arranged values, it is noticeable that there are differences in the dynamics, since the outputs do not converge to linearly ordered values. For this reason, parameters corresponding to each of the curves were estimated using MATLAB System Identification Toolbox. The parameters of the transfer function (Eq. 7) for their respective responses to the steps are listed at Table 1.

Table 1. Parameters for each step response.

	$FT_1(20\%)$	$FT_2(40\%)$	$FT_3(60)\%$	$FT_4(80\%)$
$\boldsymbol{a}$	$2,0862 \times 10^{-5}$	$2,5570 \times 10^{-5}$	$2,1716 \times 10^{-5}$	$2,0938 \times 10^{-5}$
$\boldsymbol{b}$	$1,8816 \times 10^{-2}$	$2,5726 \times 10^{-2}$	$2,1689 \times 10^{-2}$	$2,1360 \times 10^{-2}$
$\boldsymbol{c}$	$1,0341 \times 10^{-4}$	$1,4063 \times 10^{-4}$	$1,1083 \times 10^{-4}$	$9,8060 \times 10^{-5}$

6. NONLINEAR MODEL

As discussed in Section 5, the four responses to the steps have different dynamics and therefore, each of them has been synthesized by estimating the parameters *a*, *b* and *c*, composing four different transfer functions. Thus, the computational mathematical model developed to encompass the maximum of these characteristics of the real plant is able to vary *a*, *b* and *c*, according to the input value U (s). For U (s) values between 0 and 20% and between 80 and 100 %, transfer functions 1 and 4 are used, respectively. For intermediate values, that is, values of U(s) between the nominal values that produced each transfer function, a linear interpolation of the parameters is calculated. The block diagram of Figure 6, designed in SIMULINK, condenses the above-mentioned characteristics.

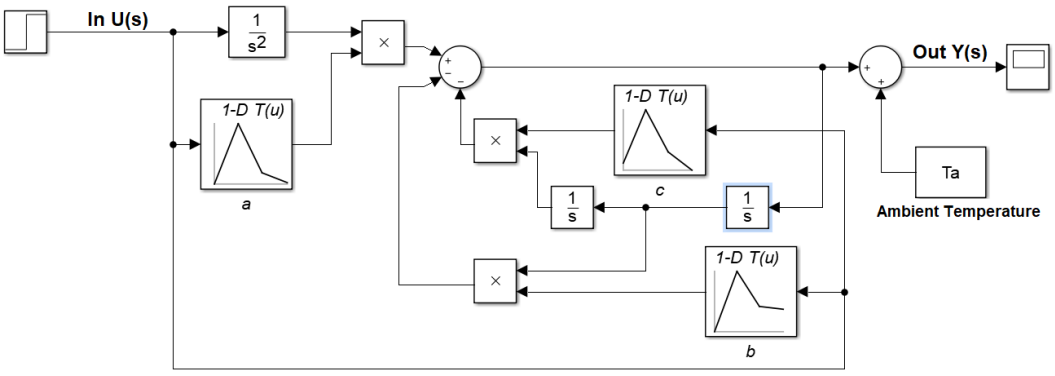

Figure 6. SIMULINK nonlinear model.

To establish the validation of the present model, tests with intermediate steps values were performed: 30, 50 70 %. These steps were applied to both the actual plant and the model of Figure 6. The graphical comparison is presented below in Figures 7, 8 and 9.

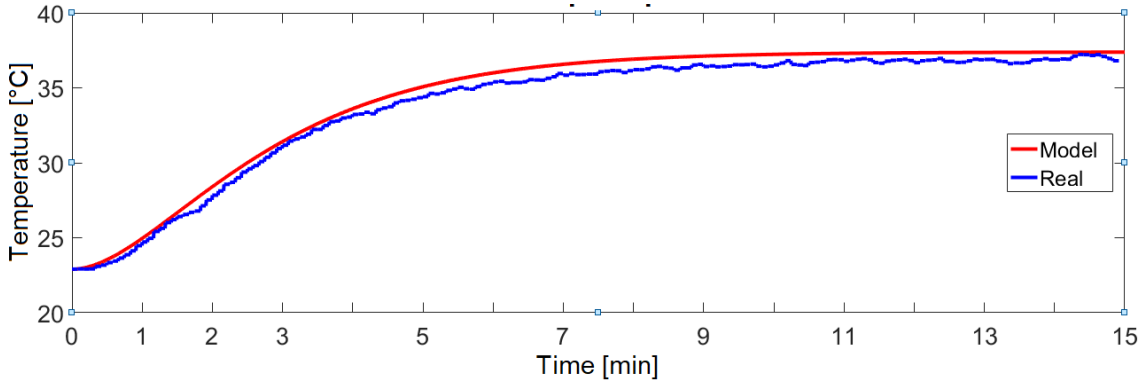

Figure 7. 30% Step response.

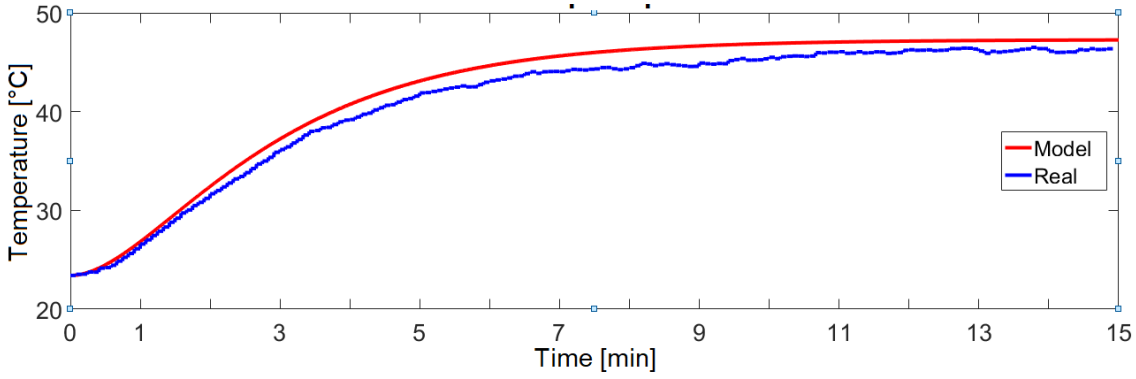

Figure 8. 50% Step response.

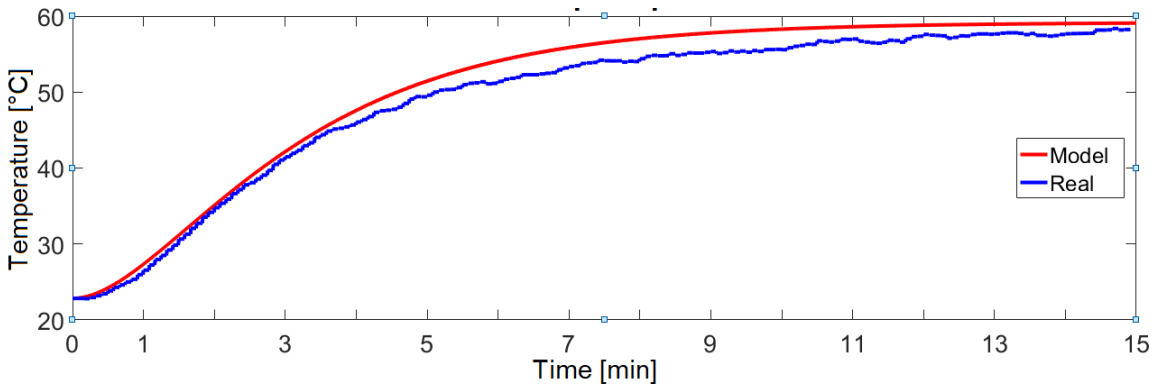

Figure 9. 70% Step response.

As presented in the graphs of Figures 7, 8 and 9, the dynamics of the real system were well absorbed by the developed mathematical model. Having a mathematical computational model that well represents the actual plant, the controller can be synthesized with all the security and speed that SIMULINK simulations provide.

7. CONTROL

Since the nonlinear model represents a second-order system whose parameters vary linearly between four relatively similar references, according to the input applied, a fixed-gain PI controller was sufficient to meet the project control specifications, as shown below. The nonlinear model can be expressed by the transfer function of Eq. 7, whose parameters *a*, *b* and *c* vary according to input U(s) of the plant.

The performance specifications are:

I. Steady-state error (e_{ss}) null;
II. Settling time (T_s) less than 15 minutes;
III. Overshoot (M_p) less than 10%.

First, the performance of a possible proportional gain controller K_p was analyzed. However, as is proved below, a simple closed-loop system with a proportional controller does not meet the e_{ss} specification. According to the Final Value Theorem (Ogata et al., 2002):

$$e_{ss} = \lim_{s \to 0} sE(s) \tag{8}$$

Observing the steady-state error for a unit step reference:

$$e_{ss} = 1 - \left(\frac{aK_p + cT_a}{aK_p + c(T_a + 1)} \right) \tag{9}$$

Since *a*, *c* and T_a are all real numbers greater than zero, no matter the value of K_p, the steady-state error will always be greater than zero.

In order to eliminate the steady-state error, an integrative gain K_i is added to the *C(s)* controller:

$$C(s) = K_p + \frac{Ki}{s} \tag{10}$$

In order for the system to be stable, the values of K_p and K_i must be in the K_p X K_i plane delimited by the lines obtained through the Routh-Hurwitz Stability Criterion (Franklin et al., 2009).

$$\begin{array}{c|cc} s^3 & 1 & aK_p \\ s^2 & b & aK_i \\ s^1 & \frac{b(aK_p+c)-aK_i}{b} & 0 \\ s^0 & aK_i & 0 \end{array} \tag{11}$$

Since a, b and c vary, five different conditions were created, as shown at Figure 10. Based on these conditions, we can delineate the values of K_p and K_i for which the system is stable. Once the stability region has been established, K_p and K_i are bounded to the first specification. Then, a second region belonging to the stability region was delimited and analyzed regarding the remaining two specifications: $M_p < 10\%$ and $T_s < 15min$. Therefore, the parameter region K_p and K_i of Figure 11 has been defined.

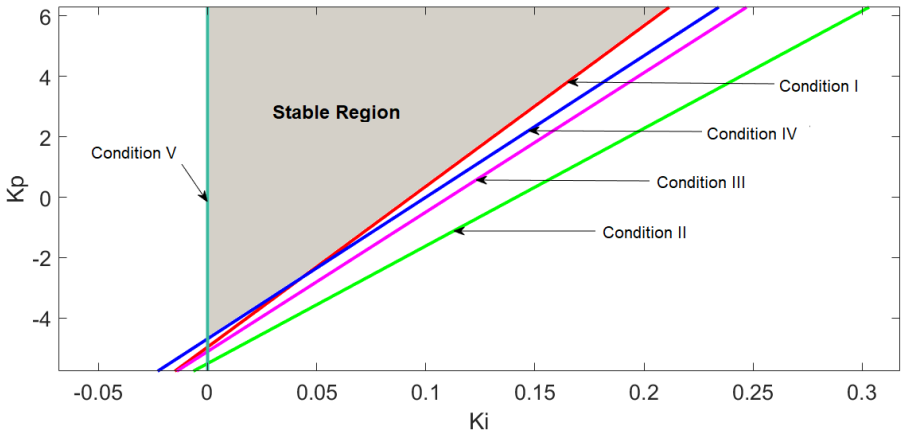

Figure 10. Stability region.

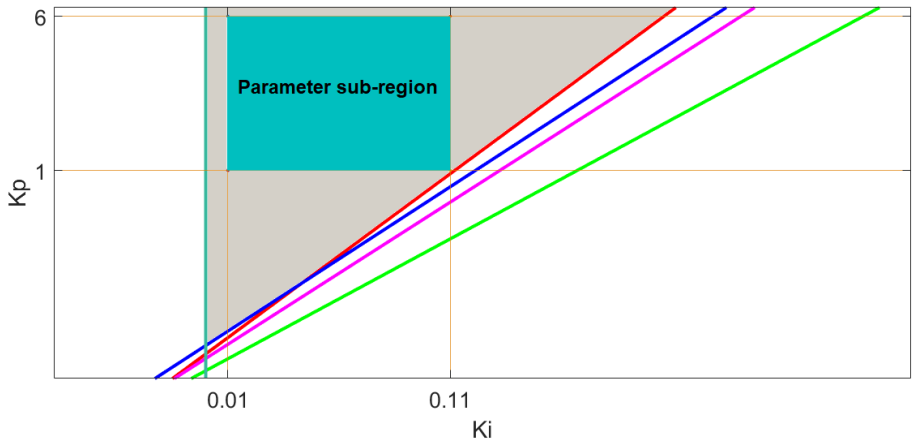

Figure 11. Parameter sub-region.

In the sub-region delimited in Figure 11, 121 simulations were done, each one with a different combination of parameters. The control parameter K_p was varied monotonically between 1 and 6, with step of 0.5. While K_i was varied the same way, but between 0.01 and 0.11, with step of 0.01. Thus, for each control parameter, in the sub-region of Figure 11, 11 different values were chosen and, in combination, provided the 121 simulations. The scheme of Figure 12, created in SIMULINK, was used for the simulations of combinations of the above control parameters.

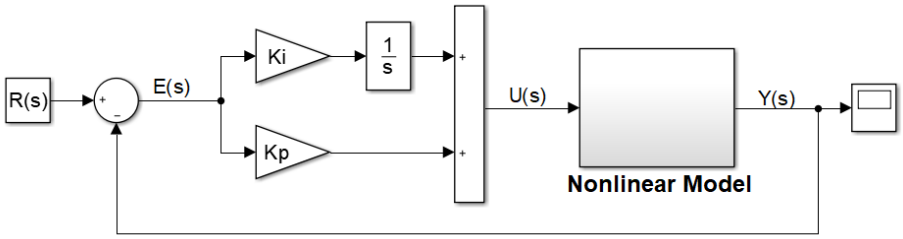

Figure 12. SIMULINK BD for simulation.

Although they may contain the information, tables, by themselves, are not visually suggestive. Therefore, graphical tools were used instead, in order to reveal trends more holistically. The surfaces (Figure 13), where M_p and T_s, calculated for each simulation, are normalized around their minimum specifications.

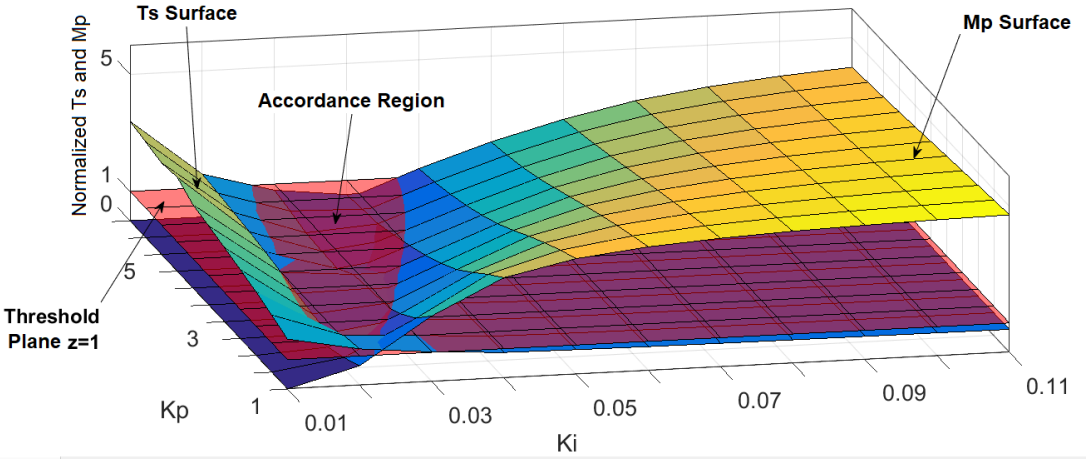

Figure 13. Performance surfaces.

As can be seen in Figure 13, the Accordance Region, as referred to in this work the region of the K_p X K_i plane where all specifications are met, is created from the intersection of the three present surfaces, being located only where the threshold is larger than the two other surfaces. With the Accordance Region, the combination of parameters that best met the specifications was chosen for the implementation of the controller in the real plant. The curve in Figure 14 shows the simulated performance of the controller that best met the specifications. The reference was 55°C. In addition to meeting the specifications, the controller performance with the gains $K_p = 5$ and $K_i = 0.03$ was perfect from the overshoot viewpoint and approximately 50 % better than the minimum required for T_s.

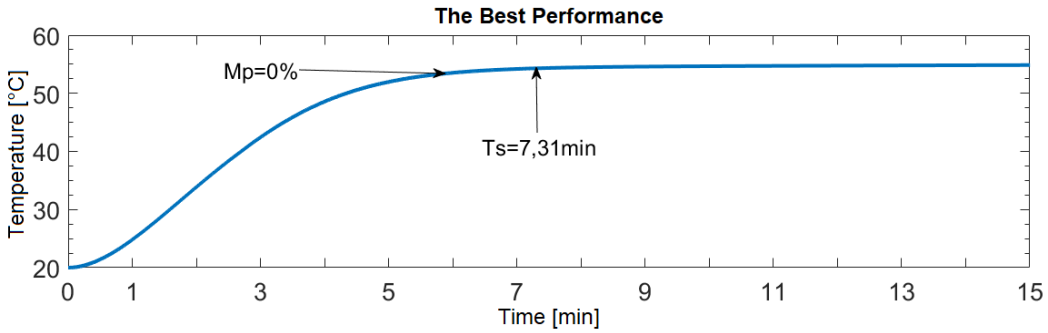

Figure 14. Best simulated controller.

This controller has been implemented through the HIL configuration illustrated by the diagram of Figure 3.The scheme developed in the SIMULINK used for implementation of the controller is set out in Figure 15.

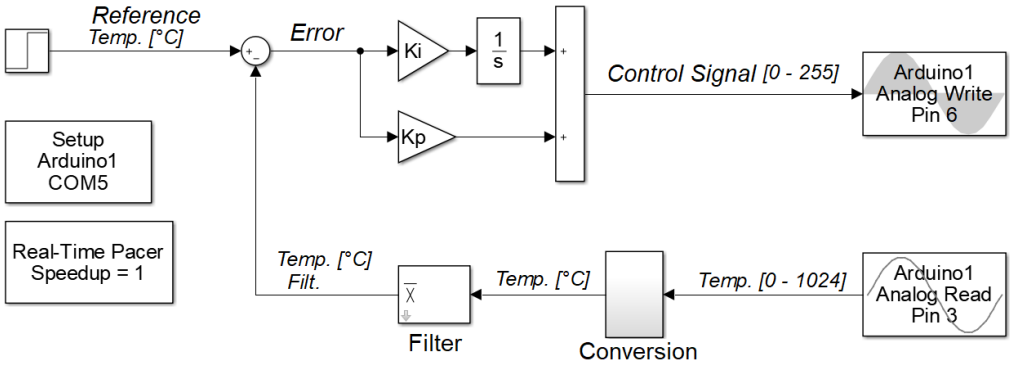

Figure 15. SIMULINK implementation BD.

The result of the implementation, considering the accuracy limitations of the temperature sensor (0.5°C) and resolution of the Arduino Uno A / D converter (10 bits), met expectations. Figure 16 illustrates the response of the simulated and the real systems to a reference of 55°C.

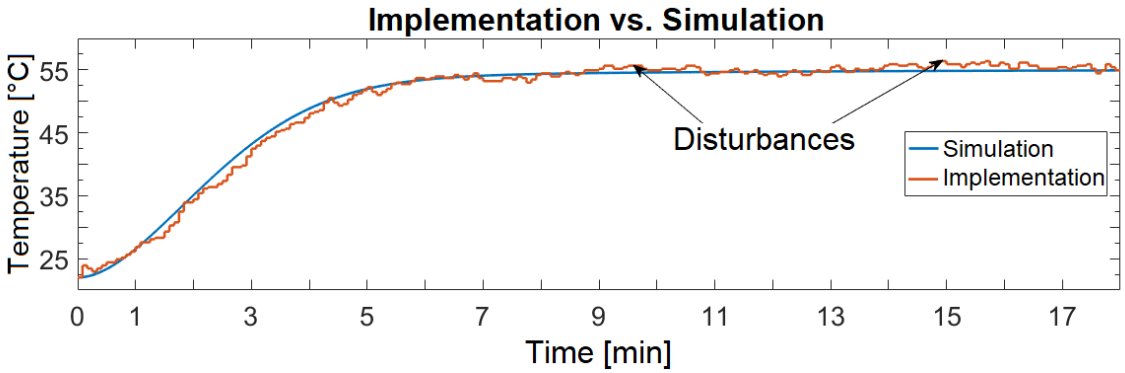

Figure 16. Implementation vs. Simulation.

8. RESULTS

From the standpoint of performance, the product achieved exceptional results. Dehydration tests also revealed, however, a different rate of evaporation between the trays. The first test was carried out with the purpose of measuring the dehydration capacity in general, therefore, the dehydrated substance was the mineral water. The choice of this material avoided the interference of other factors that could bias the results, since each food has a different propensity to dehydration. At the end of the experiment, which dehydrated 300ml of water, only the mineral salts that were dissolved in the liquid remained in the trays. The water was equally divided between the three trays, the time it took each to complete the process is listed in Table 4.

Table 2. Test I.

Desidratação de 300ml de água mineral a 55°C		
Bandeja	Tempo	Quantidade
Superior	2h e 43min	100ml
Mediana	1h e 25min	100ml
Inferior	1h e 55min	100ml

From the performance of each, it is concluded that the dehydration in the Lower Tray is 1.42 times more powerful than the Superior, and the Medium is 1.92 times more powerful than the first. Therefore, these proportions must be obeyed when calculating the amount of food that will be dehydrated in each of them. In order to verify this assumption, a second test was performed. The operating temperature was 55°C, as in the first test. The results are documented in Table 3, below:

Table 3. Test II.

Desidratação de 450ml de leite a 55°C		
Bandeja	Tempo	Quantidade
Superior	3h e 03min	100ml
Mediana	3h e 08min	200ml
Inferior	3h e 04min	150ml

From Table 3, it was concluded that the proportions of the first test were applied to the second, since the drying times were approximately the same when in this case the amount of material was calculated according to the power of each tray. In addition, it is interesting to note that in the Upper Tray there was a 20min difference between the drying of the water and the milk. This is expected, since each food has a different chemical composition and thus a different evaporation rate.

9. CONCLUSION

A dehydrator chamber with temperature control was built successfully. The project of the chamber was designed to provide a simple and inexpensive construction. Elementary techniques and tools were used in the mechanical construction part, which produced an aesthetically and functionally satisfactory prototype. The actuators, sensors and other components of the electrical circuit were chosen according to the needs of the project, which were not very sophisticated, they demanded simple and easy replacement items. These characteristics made the chamber have a very low cost of production compared to the commercially available models. The temperature control, essential in a dehydrating chamber, was conceived in four steps: thermal modeling, parameter identification, creation of a model for simulation and controller design. Once implemented, the control remained in operation for about 6 hours of testing, without any problem; concluding, so that it was implemented successfully. Finally, the dehydration tests showed that the equipment works according to expectations. With the dehydrator chamber operating exactly as expected, the next steps are summarized in the preparation of this product for commercial use. First, the controller will be shipped on a microcontroller to make the equipment independent of the use of a dedicated PC. This will also require the creation of an HMI for setting the setpoint and monitoring the temperature. In addition, the components will be physically arranged in order to provide greater mechanical robustness to the future operating environment.

10. REFERENCES

Brian, A. Historical origins of food preservation. *National Center for Home Food Preservation| NCHFP Publications, Athens*, 2002.

Close, C. M.; Newell, J. C.; Frederick, D. K. *Modeling and analysis of dynamic systems*. [S.l.]: Wiley, 2002.

Fellers, C. R. Public health aspects of food preservation. *American Journal of Public Health*, American Public Health Association, v. 17, n. 5, p. 470–475, 1927.

Fellows, P. J. *Food processing technology: principles and practice*. [S.l.]: Elsevier, 2009.

Fotek. *DC to AC Solid State Relay*. [S.l.], 2016. Available at: <http://www.fotek.com.hk/solid/SSR-1.htm>. Accessed on: 02 mar. 2018.

Franklin, G. F. et al. *Feedback control of dynamic systems*. [S.l.]: Pearson Education, Inc., Upper Saddle River, New Jersey, 2009. v. 6.

Ogata, K.; Yang, Y. *Modern control engineering*. [S.l.]: Prentice hall India, 2002. v. 4.

Texas Instruments. *LM35 Precision Centigrade Temperature Sensors*. [S.l.], 2017. Available at: <http://www.ti.com/lit/ds/symlink/lm35.pdf>. Accessed on: 02 mar. 2018.

TSM Products. *Stainless Steel Food Dehydrator Operating Manual*. [S.l.], 2011. Available at: <https://www.hayneedle.com/images/pdf/smk024.pdf>. Accessed on: 01 mar. 2018.